Use of Laser Guide Star with Pyramid Wavefront Sensor

Célia Blain[a], Simone Esposito[a], Enrico Pinna[a], Alfio Puglisi[a], and Guido Agapito[a]

[a]Osservatorio Astrofisico di Arcetri, INAF, Largo Enrico Fermi, 5, Firenze, Italy

ABSTRACT

Laser Guide Star (LGS) reference sources, artificially generated at an altitude of 90 km at the atmospheric sodium layer, are mandatory to ensure large sky coverage of astronomical Adaptive Optics (AO) systems developed for 8m and Extremely Large Telescope (ELT) class telescopes. As a result of the projection effect of an object located at a finite distance from the telescope, the AO wavefront sensor (WFS) perceives the LGS as elongated. This elongation is a few arcseconds for the 8m class telescopes and can be more than 10 arcseconds for the ELTs. This can pose several challenges when using a Shack-Hartmann wavefront sensor (SHS) such as truncation effects, the requirement for large detectors, and/or the requirement for detectors with geometry that corresponds to the source shape. In this work, we report the results of numerical simulations focused on the pyramid wavefront sensor (PWFS) sensitivity when used with a LGS, in this case, a 2D extended object. In addition, the closed-loop performance of both PWFS and SHS are estimated.

Keywords: Adaptive Optics, Pyramid Wavefront Sensor, Shack-Hartmann Wavefront Sensor, Laser Guide Star, Spot Elongation.

1. INTRODUCTION

Extensive simulations, laboratory experimentation and on-sky testing have been done for SHS used with LGS. Many algorithms (WCoG,[1] Correlation,[2] Match Filter[3]) have been developed to optimise the spot centroid estimation when spot elongation and inhomogneity are encountered with SHS.

The potential of pyramid wavefront sensors[4] (PWFS) for next generation instruments is emphasized by the AO community. While PWFS and SHS loose part of their advantage when working with an extended object, using a PWFS could be advantageous for the following reasons:

– PWFS require less pixels than SHS using the Center-of-Gravity (CoG) spot location estimation. This is particularly relevant for ELTs where lowering the requirement on the number of CCD pixels would be beneficial for the future generations of AO instruments. Indeed, a 60 by 60 subaperture system with 10 by 10 pixel per subaperture would require a 600 by 600 pixel CCD. The current CCDs imager typically being used in WFS have 240 by 240 pixel so reducing the necessary number of pixels could greatly relax future CCD technical specifications.

– The PWFS Field-of-View (FoV) is adjustable during the observation by simply changing the field stop size. Again, using a PWFS would allow the use of a large pyramid optics instead of a very large CCD.

– Using a PWFS could reduce the negative impact of the spot elongation effect. Indeed, for SHS and PWFS, the extended object size will reduce the sensitivity, but the PWFS will not introduce any spot truncation effects typically encountered with SHS.

As a result, a better understanding and estimate of PWFS performance when used with a LGS is critical to evaluate the feasability and improvement that such a wavefront sensor could bring to the next generation instruments of 10 and 30-meter class telescopes.

Further author information: (Send correspondence to Célia Blain.)
Célia Blain: E-mail: cblain@arcetri.astro.it, Telephone: +39 055 275 2303
Simone Esposito: E-mail: esposito@arcetri.astro.it, Telephone: +39 055 275 2309

2. SIMULATING AN ELONGATED LASER GUIDE STAR

2.1 LGS elongation

On sky, the laser guide star is obtained by projecting, from the center or the side of the telescope primary mirror, a sodium laser tuned at the wavelenght of 589nm. The inhomogenous sodium layer surrounding the Earth is located at an altitude of approximately 90 km and can vary in thickness between 10 and 20 km at the zenith. Due to the projection effect, the layer thickness increases as the telescope points away from zenith.

The laser interaction with the sodium layer results in a vertically elongated spot. The maximum spot elongation in a SHS subaperture can be computed (in rad) using Eq. 1 where D is the telescope diameter, Δh is the layer thickness, and h is the layer altitude*.

$$Elongation \text{ (side launch)} = \frac{D * \Delta h}{h^2} \tag{1}$$

Thus, depending on the size of the telescope aperture and the LGS launch location, the LGS extension can vary, at zenith, from approximately 1" (8-meter telescope, center launch, 10km thick layer located at 90 km altitude) to 15" (30-meter telescope, side launch, 20 km thick layer located at 90 km altitude).

New IDL/GPU-based simulation tools have been developped, buidling on the work[56] previsously done at Arcetri Observatory, focused on the evaluation of PWFS behavour and performance comparison with SHS when setup with a LGS. The extended object is simulated by a fine array of points spread over the extended object's FoV (see Fig. 1). The simulation allows the creation of an object with 2 or 3 dimensions, with the third dimension corresponding to the vertical elongation of the object due to the thickness of the sodium layer.

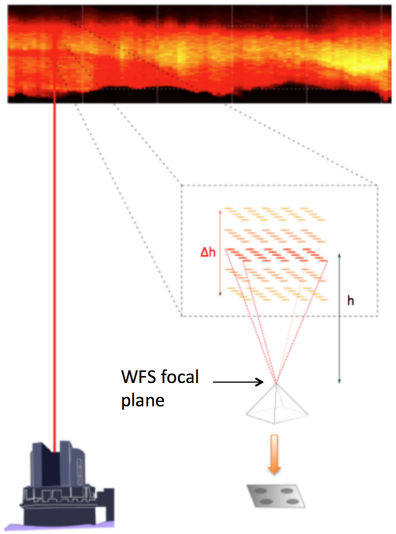

Figure 1. Diagram of a pyramid WFS used with an extended object.

The simulations presented in this paper consist of two parts and use the modal Karhunen-Loeve (KL) base.

First, the sensitivity of the PWFS was estimated, the goal was to define the impact of modulating the pyramid over its sensitivity performance: (i) locally, the sensitivity of each given point of the extended object is estimated

*For a center launch, D must be replaced by $D/2$.

individually and sensitivity maps are obtained (see Fig. 2), and (ii) globally, the sum of the sensitivity of the object's points is estimated.

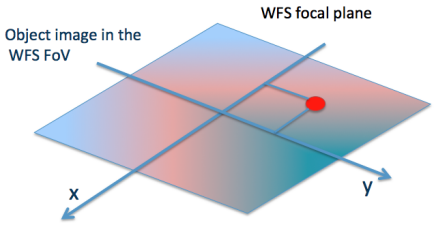

Figure 2. Sensitivity estimation for each individual point of the extended object.

Secondly, both PWFS and SHS have been used in end-to-end closed-loop (CL) simulations and their performance and noise propagation coefficients have been obtained. In the following, we describe the parameters used for the simulations described above.

2.2 Simulation parameters

The results presented in Sec. 3 and 4 have been obtained with a 2D horizontally extended object on a 8-meter class telescope. Due to the large number of points used to represent the object and to the computationally intensive computations involved, using a GPU is mandatory.

In order to sufficiently sample the extended object, a grid of 55 by 55 points was used. The extended object's Full-Witdh-Half-Max (FWHM) is 1". The WFS FoV is set to 5" in order to avoid aliasing effect due to padding in the simulations. The modes 3, 50, 100 and 600 of the KL modal base are used. The modulation amplitude applied varies from 0 to $10\lambda/D$ (with D = 8m). We ran the simulations with both Uniform and Gaussian illuminations. However, the results for both illuminations are very similar and, therefore, we only present results obtained with a Gaussian illumination. There are 40 sub-apertures accross the pupil (this configuration will be implemented in the next 3-5 years on the next generation of VLT and LBT instruments) with a sampling frequency of 800 Hz. The parameters used in the simulation are summerized in Tab. 1.

3. PYRAMID WAVEFRONT SENSOR SENSITIVITY

3.1 Local sensitivity

To estimate the sensitivity of the PWFS when using a LGS, a positive KL mode is applied and the PWFS signals are measured for each point of the extended object. The PWFS signals are obtained by computing the difference between the 4 quadrants (indicated by the green numbers in Fig. 9) as shown in Eq. 2 and 3.

$$S_x = \frac{I_2 + I_4 - I_3 - I_1}{\sum_{i=1:4} I_i} \tag{2}$$

$$S_y = \frac{I_1 + I_2 - I_3 - I_4}{\sum_{i=1:4} I_i} \tag{3}$$

The same measurement is reproduced with the equivalent but negative KL mode and for each point, the rms of the difference between the positive and negative signals obtained are recorded.

Table 1. General parameters used in the simulations.

Telescope Diamter D	8 m
Grid size	55 x 55
Number of layers	1
Object FWHM	1”
WFS FoV	5”
Illumination	Gaussian
Wavelength	589 nm
Modal base	KL (mode: 3, 50, 100, 600)
Max number of modes (for IM computation)	600
Modulation amplitude	0 to 10λ/D
Flux	Rmag=10 equivalent LGS
Number of subapertures	40 x 40
Sampling frequency	800 Hz

The values of the resulting sensitivity rms for every point is then displayed as a 3D map. The sensitivity estimation is repeated for mode 3, 50, 100 and 600 with and without modulating the PWFS.

The resulting sensitivity 3D maps are presented in Fig. 3 to 6. In all figures, the vertical scale extends from 0.02 to 0.4 rms with the lower values being represented in blue and the higher values being represented in red.

3.1.1 Without modulation

Without modulating the PWFS (Fig. 3), at low order modes, the pyramid is mostly sensitive at the apex and along the edges. As the mode's order increases, the sensitivity of points located father from the apex and edges starts to rise.

3.1.2 With modulation

When the pyramid is modulated (Fig. 4, 5 and 6), the increase in the mode's order is also accompanied by an increase in the WFS sensitive area. However, another effect can be seen: the apparition of regions of maximum sensitivity which do no follow the edge areas. This effect is not necessarly intuitive and in the following, a simple case of a tilt will be used to explain the 3D maps obtained.

3.1.3 Off-axis point's sensitivity with a tilt applied

In Fig. 4-6, one can see that the modulation of the pyramid results in the apparition of peculiar vertical and horizontal linear patterns. Unlike the case without modulation where the maximum sensitivity is obtained along the edges and at the apex, with modulation, it appears that the areas of maximum sensitivity follow new lines, parallel but shifted from the edge. This is particularly visible on Fig. 4 where a low order mode (mode 3) is applied. The areas of maximum sensitivity (represented in red) are located in 4 distinctive points. The distance from these points to the pyramid apex increases with the modulation amplitude. The vertical and horizontal lines of maxima are parallel to the axis and pass through these 4 points.

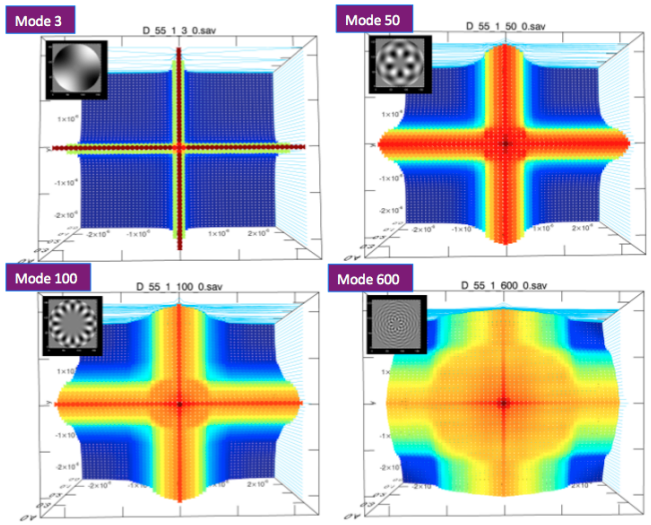

Figure 3. 3D maps of the PWFS sensitivity for KL mode 3, 50, 100 and 600 when the pyramid is not modulated. The mode is shown in the the black and white image on the top-left corner of each individual 3D map.

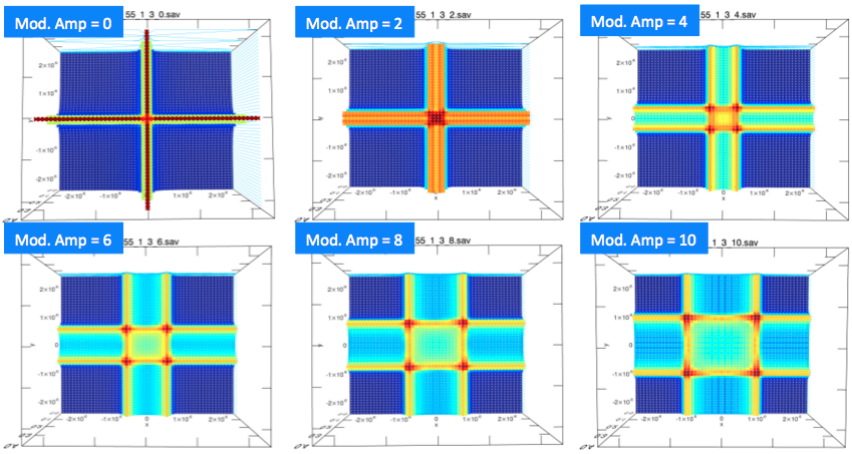

Figure 4. 3D maps of the PWFS sensitivity for KL mode 3 when the pyramid is modulated from 0 to 10λ/D.

To understand this effect, let's consider the case where the mode applied is a simple tilt δx. The sensitivity map obtained when measuring the signal S_x (corresponding to an horizontal spot displacement) is shown in Fig. 7. The modulation amplitude is 4λ/D.

Fig. 8(left) represents the case of an on-axis point. The pyramid edges are represented in blue. The on-axis point is located at the apex of the pyramid and a modulation of radius R_M is applied. The path followed by the on-axis point during the modulation is represented by the purple circle and this path defines the pyramid signal output. When a tilt is applied, the point's location become shifted by δx. For simplicity, we choose δx to be to the right along the horizontal edge. When the pyramid is modulated, the path followed by the tilted point is now indicated in yellow and the signal output by the pyramid corresponds to the light path shown along the red

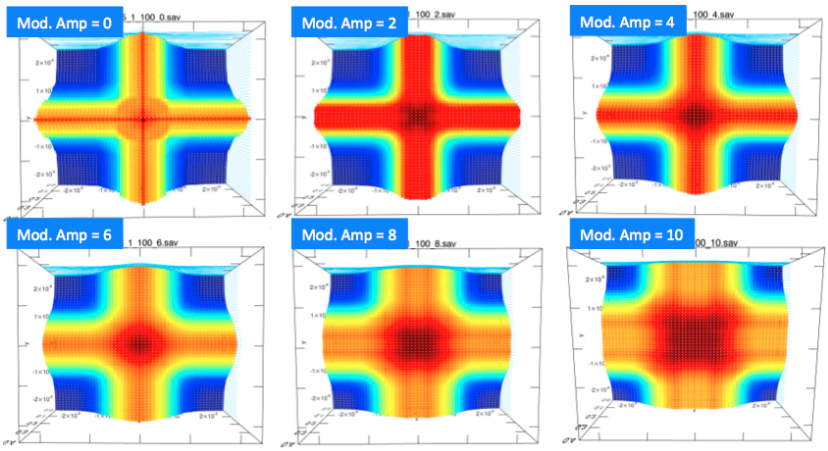

Figure 5. 3D maps of the PWFS sensitivity for KL mode 100 when the pyramid is modulated from 0 to 10λ/D.

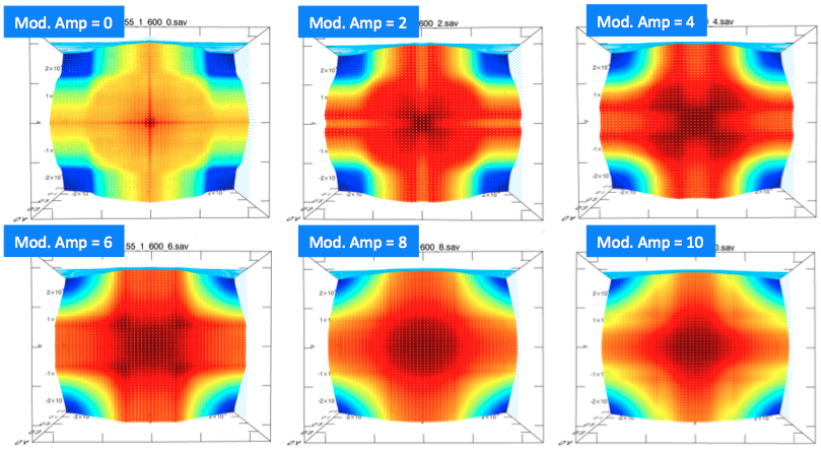

Figure 6. 3D maps of the PWFS sensitivity for KL mode 600 when the pyramid is modulated from 0 to 10λ/D.

arrows.

For an off-axis point, represented in Fig. 8(right), the point location is defined by the distance OA to the apex. The modulation path followed by this point when modulated is the pink circle. When a tilt is applied, the off-axis point location is shifted by δx and the new modulation path followed is shown in yellow.

In Fig. 9, a more detailed diagram of the sensitivity estimation for a given tilt applied at a certain off-axis point (here represented in black) is presented. A positive tilt δx is applied (red point and corresponding modulation path) and the pyramid measurements S_x and S_y (Eq. 2 and 3) are recorded. Then a negative tilt -δx is applied (orange point and corresponding modulation path) and the rms of the difference between the measurements obtained with δx and -δx corresponds to the sensitivity $\varsigma_{e(i,j)}$ for the black off-axis point.

As a result, for the sensitivity estimation, the photons located within the blue rectangles on Fig. 9 (or red arrows in Fig. 8) are the photons providing the signal thus the sensitivity estimation. With respect to the y

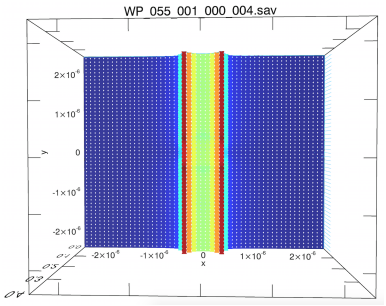

Figure 7. Sensitivity map obtained when a tilt δx is applied to the modulated pyramid while measuring the signal S_x (corresponding to an horizontal spot displacement). The modulation amplitude is $4\lambda/D$.

axis and in the case of a tilt applied along the x-axis, the signal (the difference between the number of photons within the top blue rectangle and the bottom blue rectangle) is always zero. With respect to the x axis, as the distance AO of the off-axis point from the apex increases, one can see that the PWFS signal gradually increases to a maximum value (in red in Fig. 7) reached when AO = $R_M+\delta x$, after which the signal becomes zero.

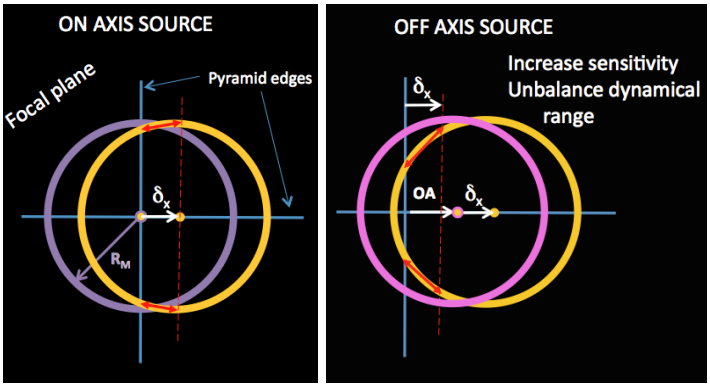

Figure 8. Diagram of an on-axis point (left) and off-axis point (right) in the focal plane, for a modulated pyramid when a tilt of δx is applied.

3.2 Overall sensitivity over the full extended object

In order to determine if the pyramid sensitivity can be improved by a given modulation amplitude, the sensitivity of each point of the extended object was summed and a global sensitivity ς_g was estimated as shown in Eq. 4 where $F_{(i,j)}$ is the flux for a given point of the extended object. ς_g was estimated for the four modes applied.

$$\varsigma_g = \sum_{i,j} \varsigma_{e(i,j)} * F_{(i,j)} \tag{4}$$

This was done at various modulation amplitudes (from 0 to $10\lambda/D$). The resulting plot is presented in Fig. 10. The plot clearly shows that modulating the pyramid does not provide any improvement for the overall sensitivity. Adding modulation greatly increases the computational weight in the simulations. As a result, the closed-loop (CL) simulations described in Sec. 4 have been performed without modulation.

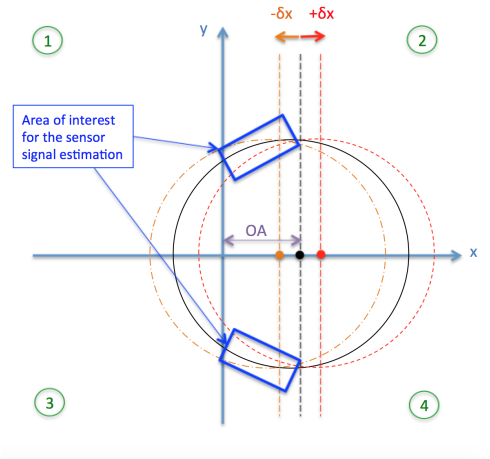

Figure 9. Detailed diagram of the sensitivity computation for an off-axis point with a tilt applied along the x axis.

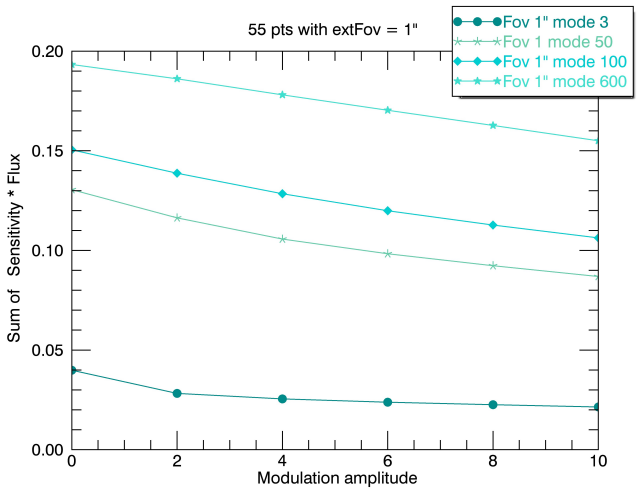

Figure 10. Global rms sensitivity ς_g versus modulation amplitude for mode 3, 50, 100 and 600.

4. END-TO-END SIMULATIONS: SHS VERSUS PWFS IN CLOSED-LOOP

In order to compare the performance of a PWFS and a SHS when a LGS is used, two sets of simulations, using matching parameters, have been run in parallel. For both simulations, the interaction matrices were recorded for a 2D horizontally extended object and used to perform 1000 closed-loop iterations under evolving turbulent conditions. The flux is set to have an equivalent magnitude 10 (R band) LGS. The parameters are summerized in Tab. 2.

The performance of both WFS compares by looking at the modal plots obtained after 1000 CL iterations. The modal plots represent the residual aberration per mode. The highest order mode used for these simulations was 600.

Table 2. Parameters used in the end-to-end CL simulations.

Extended object FoV	1”
Max number of modes	600
Number of subapertures	40 across the pupil
Seeing	0.56”
Gain	0.3
Illumination	Gaussian
Wind speed	8.6 m/s
Flux	20700 ph/frame
Noise	Photon noise

The modal plots for the PWFS and the SHS are presented in Fig. 11 and show that (i) the performance of the PWFS and the SHS are similar and (ii) the pyramid residuals for the low order modes are slightly smaller than the SHS.

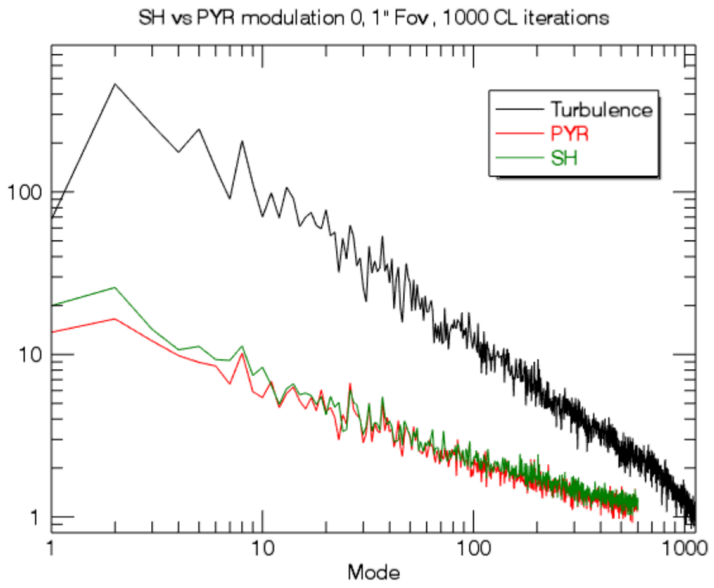

Figure 11. Modal plots of the PWFS and the SHS for 1000 CL iterations.

5. CONCLUSION AND FUTURE WORK

In this paper, we presented the results of simulations focused on evaluating the performance of a PWFS when used with a 2D elongated LGS. From the sensitivity simulations, one can see that modulating the pyramid does not improve its overall sensitivity. Closed-loop end-to-end simulations have also been performed to compare the

performances of a PWFS and a SHS when using a LGS. The results show that both sensors performed similarly with the PWFS performance being slighlty better at low order modes.

The next step will consist of reproducing the simulations presented in this paper for a 3D extended LGS, with the third dimension corresponding to the thickness Δh of the sodim layer.

REFERENCES

[1] Nicolle, M., Fusco, T., Rousset, G., and Michau, V., "Improvement of shack-hartmann wave-front sensor measurement for extreme adaptive optics," *Opt. Lett.* **29**, 2743–2745 (2004).

[2] Poyneer, L. A., "Scene-based shack-hartmann wave-front sensing: analysis and simulation," *Appl. Opt.* **42**, 5807–5815 (2003).

[3] Gilles, L. and Ellerbroek, B. L., "Shack-hartmann wavefront sensing with elongated sodium laser beacons: centroiding versus matched filtering," *Appl. Opt.* **45**, 6568–6576 (2006).

[4] Esposito, S. and Riccardi, A., "Pyramid wavefront sensor behavior in partial correction adaptive optic systems," *A&A* **369**, 9–12 (2001).

[5] Pinna, E., Puglisi, A. T., Argomedo, J., Quiros-Pacheco, F., Riccardi, A., and Esposito, S., "The pyramid wavefront sensor with extended reference source," in [*Second International Conference on Adaptive Optics for Extremely Large Telescopes*], (2011).

[6] Quiros-Pacheco, F., Pinna, E., Puglisi, A. T., Busoni, L., Agapito, G., Rabien, S., and Esposito, S., "Pyramid wavefront sensor performance with laser guide stars," in [*Third International Conference on Adaptive Optics for Extremely Large Telescopes*], (2013).